Journal of Applied Physics ARTICLE scitation.org/journal/jap

Polarization control in nitride quantum well light emitters enabled by bottom tunnel-junctions

Cite as: J. Appl. Phys. **125**, 203104 (2019); doi: 10.1063/1.5088041
Submitted: 7 January 2019 · Accepted: 3 May 2019 ·
Published Online: 30 May 2019

Henryk Turski,[1,2,a)] Shyam Bharadwaj,[1] Huili (Grace) Xing,[1,3,4] and Debdeep Jena[1,3,4]

AFFILIATIONS

[1]Department of Electrical and Computer Engineering, Cornell University, Ithaca, New York 14853, USA
[2]Institute of High Pressure Physics, Polish Academy of Sciences, Sokołowska 29/37, PL-01-142 Warsaw, Poland
[3]Department of Materials Science and Engineering, Cornell University, Ithaca, New York 14853, USA
[4]Kavli Institute for Nanoscale Science, Cornell University, Ithaca, New York 14853, USA

[a)]**Email:** henryk@unipress.waw.pl

ABSTRACT

The frozen internal polarization-induced electric fields due to broken inversion symmetry in all conventional blue and green nitride semiconductor light-emitting semiconductor quantum well heterostructures point in a direction opposite to what is desired for efficient flow of electrons and holes. This state of affairs has persisted because of the desire to have p-type hole injectors on top of the quantum well active region. Because of the internal polarization fields in nitride heterostructures, there exist four permutations of doping and polarization for the realization of such light emitters. Which permutation is the most desirable for efficient light emission? In this work, we answer this question by demonstrating a fundamentally new approach toward efficient light emission with "bottom-tunnel junctions." The bottom-tunnel junction design aligns the polarization fields in the desired direction in the quantum well while simultaneously eliminating the need for p-type contacts and allowing efficient current spreading. By preventing electron overshoot past quantum wells, it disables carrier recombination in undesired regions of the quantized heterostructures and opens up the possibility for new geometries of integrating and stacking multiple light emitters.

INTRODUCTION

Quantum well (QW) semiconductor heterostructures based on the gallium nitride (GaN) semiconductor system have made it possible to realize revolutionary photon emitters in visible and ultraviolet wavelengths.[1] The development of GaN light-emitting diodes (LEDs) has enabled semiconductor-based lighting for modern residential and industrial buildings, automobiles, and mobile electronic gadgets and has also brought lighting to regions of the world that have no direct access to electricity. The high resistivity of p-type layers arising from deep acceptor ionization energies and undesirable electric field orientations due to the prevailing quantum heterostructure design of these semiconductor materials forces the LEDs to be operated under low current injection conditions to avoid (a) losses arising from high-resistance p-type contacts and (b) overshoot of hot electrons over the quantum wells causing undesired recombination. These effects become more severe at high current injection and determine the lower limit for threshold of laser diodes (LDs). Since laser-lighting is being investigated as an energy-efficient replacement to LEDs, fresh ideas rooted in the physics of the semiconductor heterostructures are needed to achieve high efficiency photon sources for the future.

One of the most important distinguishing features of III-nitride semiconductor heterostructures is the presence of built-in electronic polarization due to the lack of inversion symmetry in the wurtzite crystal structure.[2] The difference in polarization manifests as the presence of fixed sheet charges of sheet density σ_π at heterojunctions, which by Gauss's law produce internal electric fields $F_\pi = q\sigma_\pi/\varepsilon_s$, where q is the electron charge and ε_s is the semiconductor dielectric constant. Typical polarization-induced fields are in the range of $F_\pi \sim 1$ MV/cm. Because the electrostatics of p-n junction diodes and the internal quantum efficiency (IQE) of the quantum well regions (due to the quantum-confined Stark effect) are highly sensitive to these electric fields, it is important to explore the various possible orientations and combinations of polarization-induced fields and junction fields that develop due to the depletion of carriers. For vertical LEDs, spontaneous and piezoelectric fields can

either enhance or weaken the emission performance of the final device.[3] The direction of the built-in field with respect to the direction of forward current flow in the diode is a critical parameter. Due to the large asymmetry between the conductivity of n-type and p-type GaN, almost all vertical p-n diodes are produced using n-type substrates. Lack of highly conductive p-type substrates requires n-type electron injection from the bottom n-type substrate into the quantum well active regions. Being restricted to an n-type substrate, the choice of crystal growth direction—Ga-polar vs N-polar—determines whether the polarization field in the quantum wells points in the same or opposite direction to the p-n junction field and to the direction of current flow.

It has been long believed that higher energy efficiencies are possible in nitride light emitters if the quantum well heterostructures are grown in the N-polar rather than the Ga-polar orientation. The reasons for this are discussed later—but at first glance, it may seem that the polarity of the crystal heterostructure should have no effect on the IQE of the quantum wells. After all, if one considers just "photoluminescence" from the quantum wells in undoped structures, an N-polar quantum well heterostructure is equivalent to a Ga-polar heterostructure physically turned upside down, and indeed, there is no reason to expect a difference in the IQE between the two structures. However, when a quantum well heterostructure is grown along the N-polar (000−1) direction of the crystal, it is found to have a drastically lower IQE than a structurally identical Ga-polar (0001) counterpart.[4] The reason for this remains a mystery and is unsolved to date. It is likely related to the difference in defect formation mechanics, e.g., higher layer contamination[5,6] for growths in the N-polar orientation by metalorganic vapor phase epitaxy (MOVPE) and molecular beam epitaxy (MBE),[4,7–10] due to the drastically different growth dynamics and the chemistry of the N-polar and Ga-polar structures.

Constructing LEDs (or laser diodes) requires placing the quantum wells inside the depletion region of a p-n junction diode. Now, the polarity of the diode (p-layer on the top or on the bottom called p-up and p-down, respectively) and the polarization

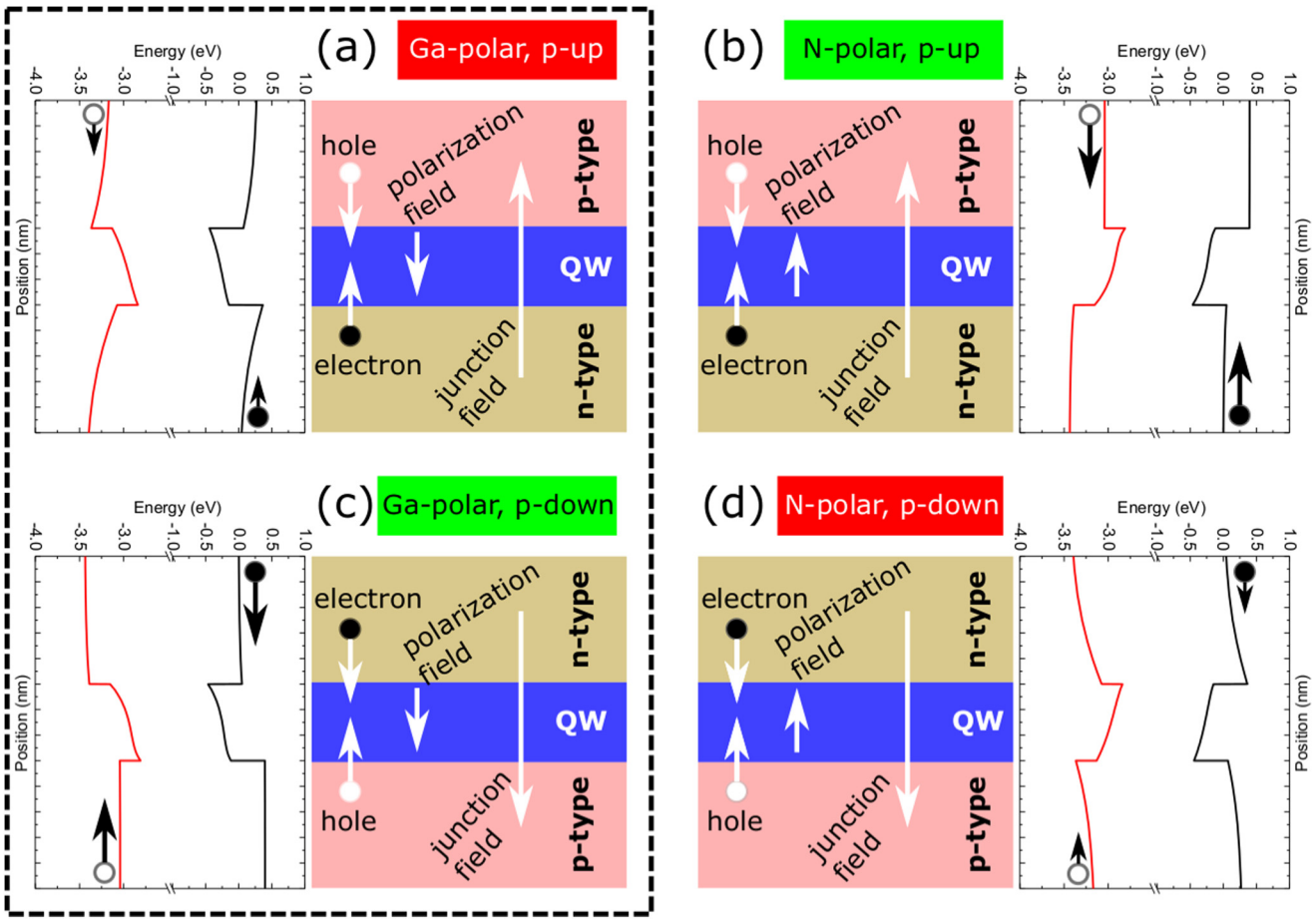

FIG. 1. Schematic image showing four different structures realizing all possible combinations of GaN crystal polarization direction and the choices of p-n junction. Next to schematic structures, corresponding band alignments under forward bias are shown. The arrows indicate electron and hole injection directions with respect to the built-in polarization fields and the doping-induced p-n junction fields. Structures under investigation in this paper are shown in (a) and (c).

of the crystal (Ga-polar or N-polar) combine to give four distinct possibilities, shown in Fig. 1. A Ga-polar structure can be p-up [conventional LED, Fig. 1(a)] or p-down [Fig. 1(c)], and a N-polar structure can be p-up [Fig. 1(b)] or p-down [Fig. 1(d)]. We will show that among these, the Ga-polar p-down [Fig. 1(c)] and N-polar p-up [Fig. 1(b)] structures are ideal for LEDs and LDs because the p-n junction field and the polarization fields are aligned. Because of the low IQE of N-polar quantum wells today, we select the Ga-polar p-down geometry [Fig. 1(c)] and experimentally prove our hypothesis that this structure has (a) much brighter light emission, (b) no carrier overflow nor undesired photon emission, and (c) excellent current spreading.

To utilize the advantages of the higher perfection of growth along the Ga-polar [0001] direction along with the preferred polarization field orientation (available for p-up LEDs grown along the N-polar [000−1] direction), tunnel junctions (TJs) must be used on n-type substrates.[11–13] Growth of such structures is complicated due to the fact that the TJ must be grown "below" the quantum well active region. This requires sustaining a high crystal quality and a smooth surface while growing highly doped p-type and n-type layers. For some applications, where a smooth surface is not crucial, this issue can be addressed by growing nanowire-based structures.[12–16] Additionally, growth of TJ structures by MOVPE is complicated, because success in effectively activate buried p-type layers is still limited[17,18] as the diffusion of hydrogen needed to activate the p-type Mg-doped GaN is forbidden through n-type GaN layers.[19,20] Hence, to realize the bottom-tunnel junction, we have chosen to use plasma-assisted MBE, a "hydrogen-free growth technique" which does not require activation of the buried p-type layer. This growth technique has been proven capable of growing high quality nitride blue laser diodes.[21]

In this paper, we analyze the impact of the direction of built-in electric field on the electrical and optical properties of MBE-grown LEDs. The desired heterostructures are realized in two varieties: by placing the TJ above the active region [top-TJ—shown in the energy band diagram in Fig. 2(a)] and below the active region [bottom-TJ—shown in the energy band diagram in Fig. 2(b)]. Electron (filled circles) and hole (empty circles) flow directions are depicted inside the LEDs under forward bias conditions. The experimentally measured current densities for such structures as a function of the external bias are shown in Fig. 2(c). As expected, the forward bias voltage direction for the bottom-TJ LEDs [as in Fig. 2(b)] is "inverted" compared to that for the top-TJ LEDs [as in Fig. 2(a)], indicating the "successful realization" of a bottom-tunnel junction LED, which makes it possible to probe the questions raised earlier. Before discussing the electroluminescence (EL) properties, we describe the details of the epitaxial growth of the heterostructures and their fabrication into LEDs.

EXPERIMENTAL

The samples shown in Fig. 3 were grown by plasma-assisted MBE on commercially available bulk n-type Ga-polar GaN substrates with threading dislocation density around 5×10^7 cm^{-2}. The composition of the active InGaN layers is chosen for two wavelengths, blue and green, and for each choice, a tunnel junction is inserted on the top and the bottom. The top-TJ structures are similar to those in prior studies[22,23] and serve as control samples, while the bottom-TJ structures are novel. The InGaN layers (in both TJ and active region) were grown at 650 °C and all GaN layers at 740 °C as measured using BandiT.[24] In each series, the samples were grown using exactly the same doping concentrations and the same alloy compositions, as indicated in Fig. 3.

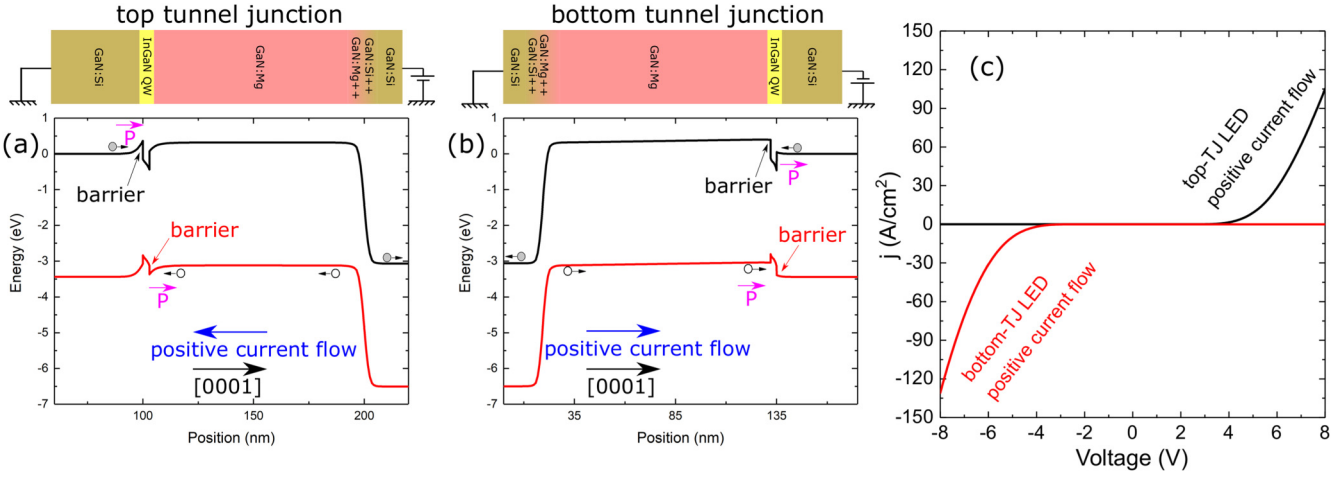

FIG. 2. Schematic energy band diagrams for forward biased single QW LEDs utilizing top-TJ (a) and bottom-TJ (b) geometries, respectively. The growth is performed in the [0001] direction, proceeding from left to right. Filled and empty circles with arrows denote carrier flow direction for electrons and holes, respectively. Polarization in the vicinity of the quantum well is marked with respect to the current flow and crystallographic [0001] direction. (c) Experimentally measured current densities as a function of external bias obtained for $80 \times 80\ \mu m^2$ LEDs utilizing the top-tunnel junction (a) and the bottom-tunnel junction (b). It is important to point out that the opposite bias direction for bottom-TJ and top-TJ structures results in the same bias applied to the LED region of both devices.

Modulation of In and Mg concentration for layers grown at the same temperature was achieved by varying atomic fluxes of Ga[25] and Mg,[26] respectively. Unintentionally doped InGaN layers in the active region were grown using a nitrogen flux of 0.9 μm/h. Only for the quantum wells for structures A and B, a growth rate of 3 μm/h was used to increase the effective indium incorporation.[25] Throughout the rest of the structure, the growth rate is kept constant at 0.35 μm/h. These rates were measured for GaN growth at 650 °C. To assure the same growth temperature for all equivalent layers, metal-desorption time measurements of reference In and Ga fluxes were performed before the growth. The surface roughness measured by atomic force microscopy (AFM) for $5 \times 5\,\mu m^2$ regions for all structures after MBE growth was below 0.5 nm indicating a smooth morphology.

In Fig. 4, high-resolution X-ray diffraction 2θ-ω scans and AFM images measured for samples in Figs. 3(c) and 3(d) are shown. They indicate successful growth of essentially identical chemical and layer compositions and thicknesses for both the top-TJ and bottom-TJ heterostructures and simultaneously prove that (a) the doping sequence has no impact on the X-ray diffraction patterns and sample morphologies and (b) the placement of the TJ at the bottom does not adversely affect the compositional control of the subsequently grown layers. As shown in Figs. 3(a) and 3(b) (structures A and B) and Figs. 3(c) and 3(d) (structures C and D), the difference between the two series is in the active region thickness and composition of the QW and barriers, composition of the electron blocking layer (EBL), and slight difference in doping levels in the TJs. The InGaN layers surrounding the active regions are used to keep the structure similar to the laser-diode heterostructure design used in our prior work.[21] Relatively thick QWs, or double heterostructure—since no quantization effects were observed, in structures C and D represent a new active region design profitable for use in LDs.[27] We also note that unlike polarization-induced heterostructure tunnel junctions,[11,19,28–33] we have chosen to use GaN:Si/GaN:Mg homojunction TJs to avoid potential complications of growing active regions on top of buried heterostructures. Single quantum well active regions were used to remove the effect of uneven carrier distribution between wells for both the blue and green LED structures to obtain a fair assessment of the impact of the built-in electric field on the intrinsic performance of LEDs for both polarities. The bottom-TJ effectively flips the LED design upside down, mimicking a N-polar p-up configuration but in the Ga-polar crystal growth orientation.

The samples were processed using optical lithography into vertical diodes of die sizes ranging from $20 \times 20\,\mu m^2$ to $300 \times 300\,\mu m^2$. Several higher aspect ratio dies were also fabricated in order to observe current spreading, with the largest aspect ratio device measuring $100 \times 500\,\mu m^2$. Inductively coupled plasma (ICP)-RIE mesa etching in chlorine based chemistry was used to isolate individual devices. Though not exploited in this work, we point out that the use of bottom-TJ structures offers a "unique advantage" of lowering the p+/n+ tunneling contact resistance by exploiting a much larger cross-section area than the LED mesa, something that is not possible in the top-TJ LED structure. After mesa isolation, a top circular Ti/Al ohmic contact of radius 25 μm for the $80 \times 80\,\mu m^2$ and larger devices was deposited at the center of the top of the mesas. Finally, a common bottom contact was deposited on the back of the n-type substrate. Prior to metallization, a surface treatment consisting of O_2 plasma ashing, HCl, and HF cleans were performed to remove undesired chemical residues. The same 25 nm Ti/100 nm Al metal stack was deposited by e-beam evaporation for both the top and bottom n-type contacts. Such a contact stack has been shown to have very low contact resistance to n-type GaN.[34]

From this point on, top and bottom-TJ samples will be compared using opposite bias directions (as indicated in Fig. 3) to enable a quantitative comparison in their natural bias conditions. The processed samples were measured on-chip by grounding the bottom contact and putting a probe on the top contact of the

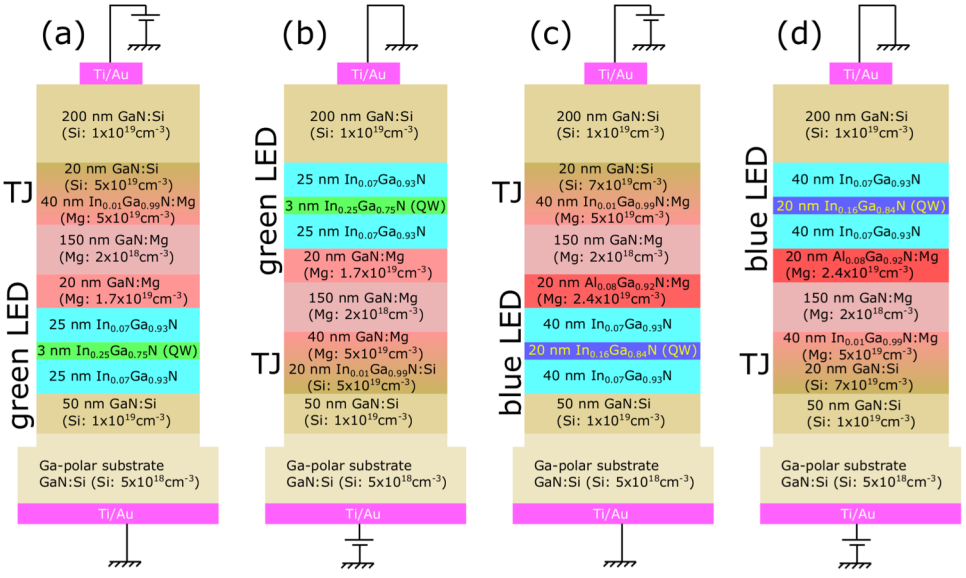

FIG. 3. Layer details of the quantum well heterostructures and doping of LEDs grown for comparison of the impact of built-in polarization-induced electric field direction. All substrates are Ga-polar. (a) and (b) have an ~25% In content 3 nm thick InGaN quantum well for green light emission, and (c) and (d) have a 16% In content 20 nm thick InGaN quantum well for blue light emission. (a) and (c) have top-TJs with an opposite junction field direction to (b) and (d), which have bottom-TJs. Structures presented in (a), (b), (c), and (d) will be referred to as A, B, C, and D, respectively. TJ and LED regions are marked for clarification.

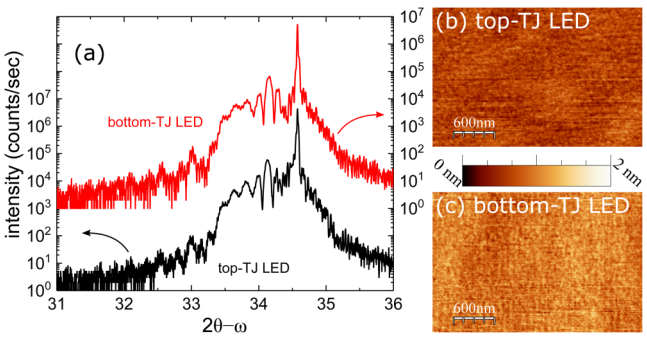

FIG. 4. (a) X-ray diffraction 2θ-ω scans obtained for structures C and D on left and right axes, respectively. The placement of the doping-induced tunnel junction on the top or the bottom has no discernible effect on the X-ray diffraction pattern. In (b) and (c), AFM images obtained for samples C and D, respectively, are presented using the same scale. Root mean square roughness obtained for $2 \times 3\,\mu m^2$ scans for both structures was 0.15 nm and 0.2 nm for top-TJ (b) and bottom-TJ (c) LEDs, respectively.

selected devices. The electroluminescence (EL) spectrum was collected from the top using an optical setup utilizing a monochromator and a photodiode.

RESULTS

The measured I-V characteristics of the four $80 \times 80\,\mu m^2$ devices are shown in Fig. 5. As expected from the comparable doping levels, current values obtained for bottom-TJ and top-TJs are at a similar level with higher values for bottom-TJ structures near the turn-on voltage [easily seen in the inset of Fig. 5(a)].

The low observed leakage levels in the reverse bias for all LED structures seen in Fig. 5 importantly indicate that the density of extended defects propagating through the LEDs in all cases is similar. This confirms high epitaxial quality of bottom-TJ structures and thereby enables a fair comparison between the top-TJ and bottom-TJ structures. The lower turn-on voltages seen in the insets of Fig. 5 for the blue LEDs whose structures are shown in Figs. 3(c) and 3(d) are due to a slight increase in the doping level in the 20 nm thick GaN:Si TJ region from 5×10^{19} to $7 \times 10^{19}\,cm^{-3}$. Theoretically, it is expected that the bottom-TJ LEDs, due to lack of barriers for current injection as indicated in Fig. 2, should profit from a slightly lower turn-on voltage. Though that is indeed the case for the measured structures, it can be deduced from Figs. 5(a) and 5(b) that a much bigger change was caused by slightly increasing doping concentration. It is important to point out that the on-resistances can be further reduced by increasing Si and Mg doping and by potentially using polarization-induced TJs with the introduction of InGaN or AlN layers in the TJ[28–30,33,35] but with a potential penalty of degraded crystal quality in the active region.

Figures 6(a)–6(d) show the measured electroluminescence spectra for the four tunnel junction LEDs. The dotted and dashed vertical lines indicate the peak emission wavelength emitted by the quantum wells at low and high excitation, respectively. The solid vertical line indicates EL associated with parasitic radiative recombination in the lower indium content InGaN layers surrounding the quantum wells, which was also reported for the TJ-less LED structure.[36] Rather interestingly, such a high energy emission peak (395–405 nm) appears for all top-TJ LEDs but "never" for the bottom-TJ LEDs. Measurements performed on different devices on

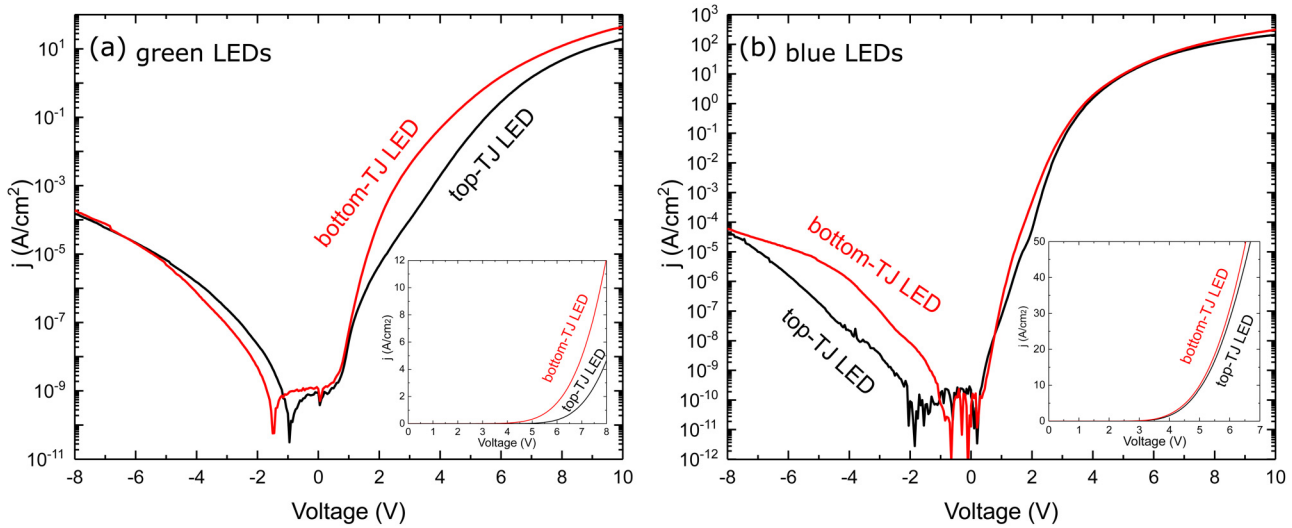

FIG. 5. Measured current density vs voltage for $80 \times 80\,\mu m^2$ devices from green LED structures (a) with top-TJ structure A and bottom-TJ structure B, and blue LED structures with (b) top-TJ structure C and bottom-TJ structure D. The insets show the same plot in the linear scale in the forward bias. The measurements show low leakage currents and the successful realization of bottom-TJ heterostructures for both the green and blue LEDs.

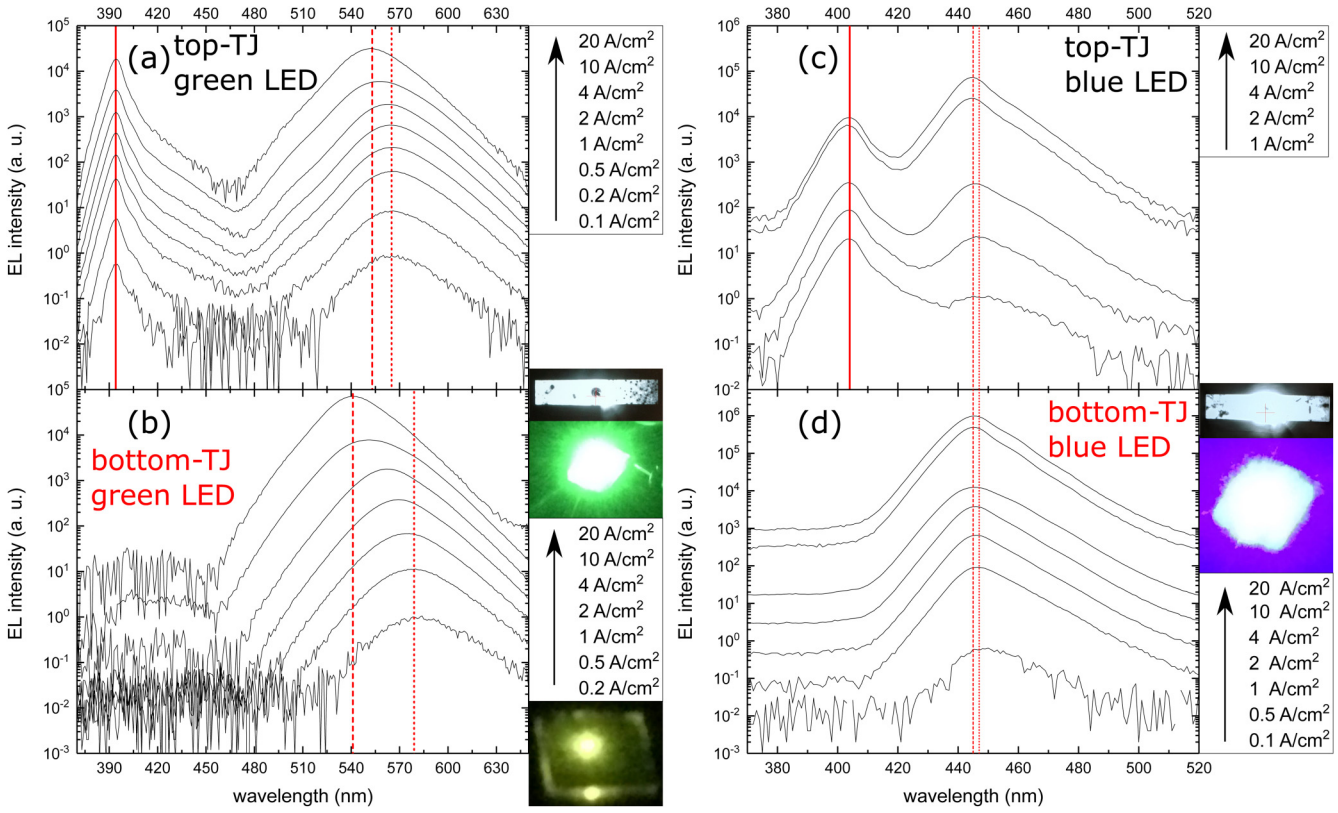

FIG. 6. (a)–(d) Electroluminescence spectra in the log scale measured on-chip for the indicated current densities for $80 \times 80\,\mu m^2$ devices of structures A, B, C, and D, respectively. A large energy emission shift is observed in (b), accompanied by real-color pictures of the whole $1 \times 1\ cm^2$ wafers next to the plot. No visible peak shift was observed for structures C and D. Above the real-color images are monochromatic images collected under a microscope for $100 \times 500\,\mu m^2$ bottom-TJ devices under 100 mA injection, showing excellent current spreading. The bottom-TJ structures B and D show single peak emission, whereas both blue and green top-TJ structures show parasitic peaks at a higher photon energy than the desired quantum well peaks.

the same sample (for top-TJ) feature slight differences in relative intensities, but the existence of the secondary peak and its dominant intensity at low current density is observed for "all" top-TJ LEDs. It is important to point out that this extra high energy peak is "not" associated with emission or reemission from the p-type doped GaN layers, as it is also measured in photoluminescence measurements of similar InGaN/InGaN QWs[37] in the "absence" of Mg-doped p-type GaN layers.

Due to the limitations of on-chip measurements, an exact comparison of the intensity between the top-TJ and bottom-TJ diodes is not straightforward due to differences in the alignment of probes. Nonetheless, at an injection current density of at 20 A/cm^2, the bottom-TJ LEDs showed ~2.5× higher peak intensity than the top-TJ for the green LEDs, and this enhancement was ~13× for the bottom-TJ blue LEDs. The quantitative differences between the enhancement for green and blue emitters can be attributed to differences in active regions and the electron blocking layer (EBL) design, but irrespective of the details, the bottom-TJ structures for both wavelengths demonstrate the important advantages offered by this conceptual change in the LED design. For the higher In content LEDs [Figs. 6(a) and 6(b)], the peak emission shifts from yellow (top-TJ: 565 nm, bottom-TJ: 580 nm) to green (top-TJ: 552 nm, bottom-TJ: 541 nm) with increasing current injection. Generally, such a shift can be attributed to either localized state filling or screening of built-in fields.[38] Since surface morphology observed after the growth of TJ, presented in Fig. 4(b), is atomically flat (at the level observed for substrates before the growth) and the same growth conditions for active regions for top-TJ and bottom-TJ structures were used, no reason for the increase in localized states creation was identified. This is why a higher blueshift for the bottom-TJ device compared to the top-TJ is a fingerprint of higher injection efficiency at high currents, leading to more pronounced localized states filling and screening of the internal polarization field. This is equivalent to say that at the same current level, the effective carrier concentration in the InGaN QW is higher in the bottom-TJ LEDs than the top-TJ LEDs, leading to more light emission.

In addition, as one can see from a comparison of Figs. 6(a) and 6(b), the blueshift in (a) occurs more abruptly at the highest current density, whereas in Fig. 6(b), it is a gradual shift with injection current. We believe that this is another fingerprint of the difference in injection efficiency between the two structures. For EL

measurements presented in Fig. 6(a) due to carrier recombination (radiative and nonradiative) taking place in the active region as well as in surrounding InGaN layers (where radiative recombination is observed), carrier density in the active region is smaller, leading to a lower blueshift.

Irrespective of the location of the TJ, all LED devices showed good current spreading: the small circular metal contact on the top was enough to spread the current throughout the entire device mesas far larger in area. Optical microscope images of the highest aspect ratio ($100 \times 500\,\mu m^2$) bottom-TJ LEDs under 100 mA

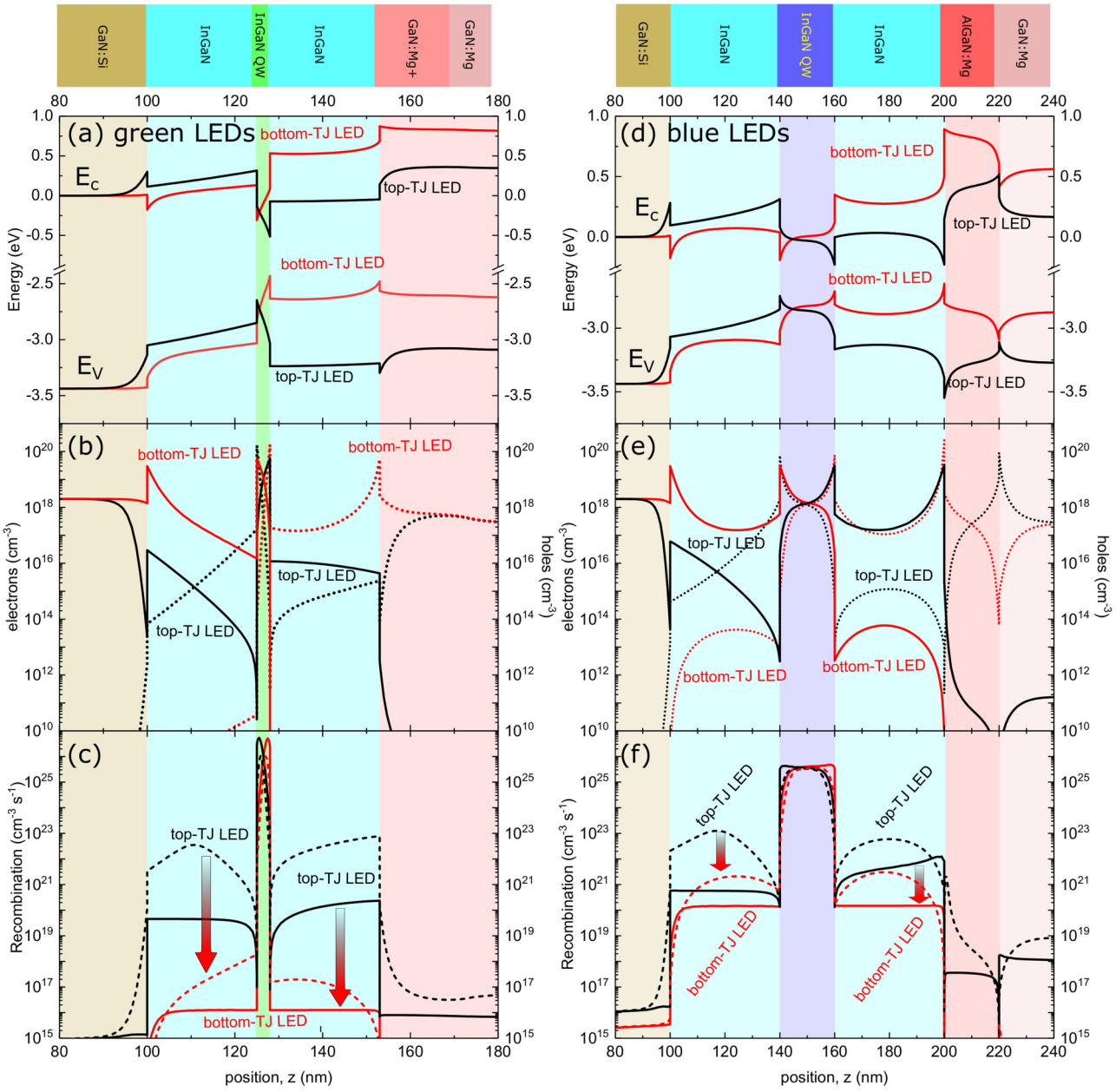

FIG. 7. Energy band diagrams, mobile carrier concentrations, and recombination as a function of position near the active region calculated by the SiLENSe package [(a)–(c)] at 20 A/cm^2 for structures A and B and [(d)–(f)] at 20 A/cm^2 for structures C and D. The results for top-TJ and bottom-TJ structures are compared. (b) and (e) Electron and hole concentrations are denoted using solid and dotted lines, respectively. (c) and (f) Differences in the radiative (solid) and Shockley–Read–Hall (SRH) non-radiative (dashed) recombination in the InGaN claddings surrounding the QW between top-TJ and bottom-TJ structures are marked with arrows.

injections are shown next to the EL spectra measurements in Fig. 6. To further analyze the origin of the high energy peak in the EL spectra for top-TJ structures, the heterostructure devices were modeled by self-consistently solving the energy band diagrams with current transport through the structure. The experimentally investigated structures utilizing top-TJ and bottom-TJ were simulated by a one-dimensional drift-diffusion model using SiLENSe: only the part of the structures marked "green LED" or "blue LED" in Fig. 3 (excluding the part denoted "TJ") were simulated, while setting the orientation as Ga-polar and N-polar, respectively. This procedure works well for modeling physical differences between the top-TJ and bottom-TJ LEDs as long as (a) the TJ resistance is low in both cases, (b) the TJ is not affected by the polarization field direction (e.g., by using a homojunction), and (c) does not degrade the LED active region quality. For simplicity, default material parameters delivered with SiLENSe were used for all presented calculations.

The calculated energy band diagrams, carrier concentrations, and radiative recombination profiles are shown in Fig. 7. These plots present results obtained at 20 A/cm^2 for the green LED structures A (top-TJ) and B (bottom-TJ) and 20 A/cm^2 for the blue LED structures C (top-TJ) and D (bottom-TJ). As seen in the energy band diagrams, the top-TJ and bottom-TJ LEDs behave quite differently under forward bias. In the top-TJ, the built-in polarization field in the QW lowers the effective band offset for electrons and holes, enabling the carriers to exit the QW and overshoot to the other side. This increases the escape of carriers from QWs, leading to higher carrier concentrations outside the QW for the top-TJ structure, compared to the abrupt drop of carrier overshoot for the bottom-TJ structure, as seen in Figs. 7(b) and 7(e). As a consequence, a significant amount of "undesired" radiative and nonradiative recombination occurs in the barriers surrounding the QW for the top-TJ structures [Figs. 7(c) and 7(f)]. For the bottom-TJ LEDs, on the other hand, due to the inverted polarization field direction in the vicinity of the QW, electrons and holes are retained in the QW and in the InGaN layer closer to the desired injection side, respectively, as seen in Figs. 7(b) and 7(e). Because of the separation of electrons and holes outside the QWs, the recombination in the barrier surrounding the QW is significantly reduced for the bottom-TJ LEDs compared to the top-TJ case [Figs. 7(c) and 7(f)]. The parasitic emission peaks seen in Figs. 6(a) and 6(c) in only the top-TJ LEDs are exactly due to this recombination in the low In-composition InGaN cladding regions and are absent in the bottom-TJ LEDs.

This change in the radiative recombination rate between top-TJ and bottom-TJ LEDs depends on the composition and thickness of the QW, barriers, and the EBL, which can be inferred from comparing Figs. 7(c) and 7(f). The simulations suggest that the bottom-TJ construction always leads to significantly "lower" undesired radiative and nonradiative recombination rates in the barriers. An important consequence of the efficient electron and hole concentration separation in the vicinity of QW is the resulting lowering of nonradiative recombination, both Shockley–Read–Hall (SRH) and Auger (less significant at shown current density levels). This fact significantly enhances the efficiency of the bottom-TJ LEDs for both low and high current densities.

The low leakage current in reverse bias seen in Fig. 5 allows a direct measurement of the capacitance-voltage (C-V) characteristics for all TJ LED samples. In Figs. 8(a) and 8(b), the capacitance values divided by device area (C/A) measured at a 5 MHz frequency as a function of forward bias of the LEDs are shown. The plots in Figs. 8(a) and 8(b) present data for the structures A and B and structures C and D, respectively. The depletion width W corresponding to the measured C/A values, assuming $W = \frac{\varepsilon_r \varepsilon_0 A}{c}$, where $\varepsilon_0 = 8.85 \cdot 10^{-8}\mu F/cm$ and $\varepsilon_r = 10$ (the electrical permittivity of vacuum and the semiconductor dielectric constant) is shown on the right vertical axes. For simplicity, ε_r is assumed to be constant for $In_{0.15}Ga_{0.85}N$ and GaN—derived from a linear extrapolation

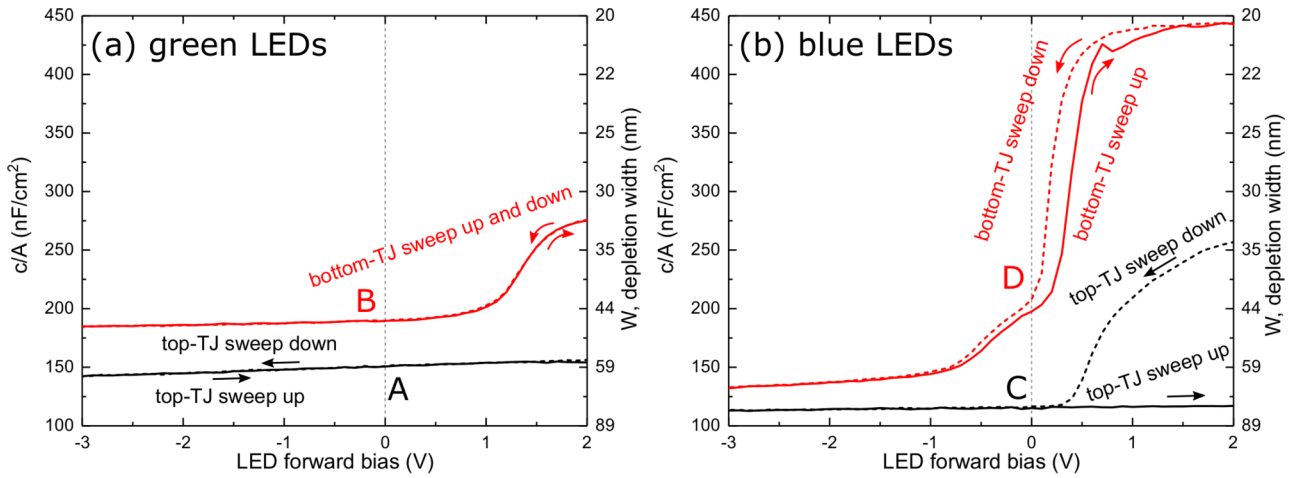

FIG. 8. Capacitance-voltage (C-V) measurements corresponding to structures (a) A and B, and (b) C and D. The higher junction capacitances as well as the minimal hysteresis observed in the bottom-TJ LEDs arise from the polarization field in the QW pointing in the same direction with the p-n junction field, which are further illustrated in Fig. 9. The C-V measurements were taken at 5 MHz.

proportional to the In content using values of 8.52 and 18.44 for GaN and InN, respectively.[39] Since the conductivity of the TJs is high, we assume that the entire measured capacitance is associated with the depletion in the LED active region. Due to the opposite orientations of the polarization-induced electric field and the p-n junction electric fields of the p-up (top-TJ) and p-down (bottom-TJ) LEDs, the chemically identical layer stacks result in remarkably different capacitances and depletion widths. As expected, W obtained for the bottom-TJ structures is significantly lower than that for top-TJ structures, implying the polarization field is aligned with the junction field, and to maintain the same net built-in field, the junction shrinks the net depletion width [see Fig. 1(b)]. This mimics the desired N-polar p-up structure [see Fig. 1(c)] in the alignment of the polarization and junction fields, but by virtue of the bottom-TJ, is effectively realized in the Ga-polar structure. For the bottom-TJ LEDs, a characteristic steep increase in the capacitance is measured for positive voltages, associated with barrier-free carrier injection and ready shrinking of the depletion regions. For example, in structure D at a forward bias voltage of ~1 V, the depletion width measured from the capacitance is essentially identical to the thickness of the QW, ~20 nm, meaning the depletion region has shrunk completely to the edges of the QW. On the other hand, a noticeable hysteresis is observed between forward and reverse voltage sweeps for the top-TJ LED, associated with charge trapping in the active region. This effect is smaller for thinner QWs and for bottom-TJ structures compared to top-TJ structures. For voltages higher than 1–2 V, the onset of current flow makes the conductance dominate over the capacitance, and the C-V measurement should not be trusted.

To benchmark the magnitude of the experimentally obtained depletion widths, energy band diagram simulations using SiLENSe

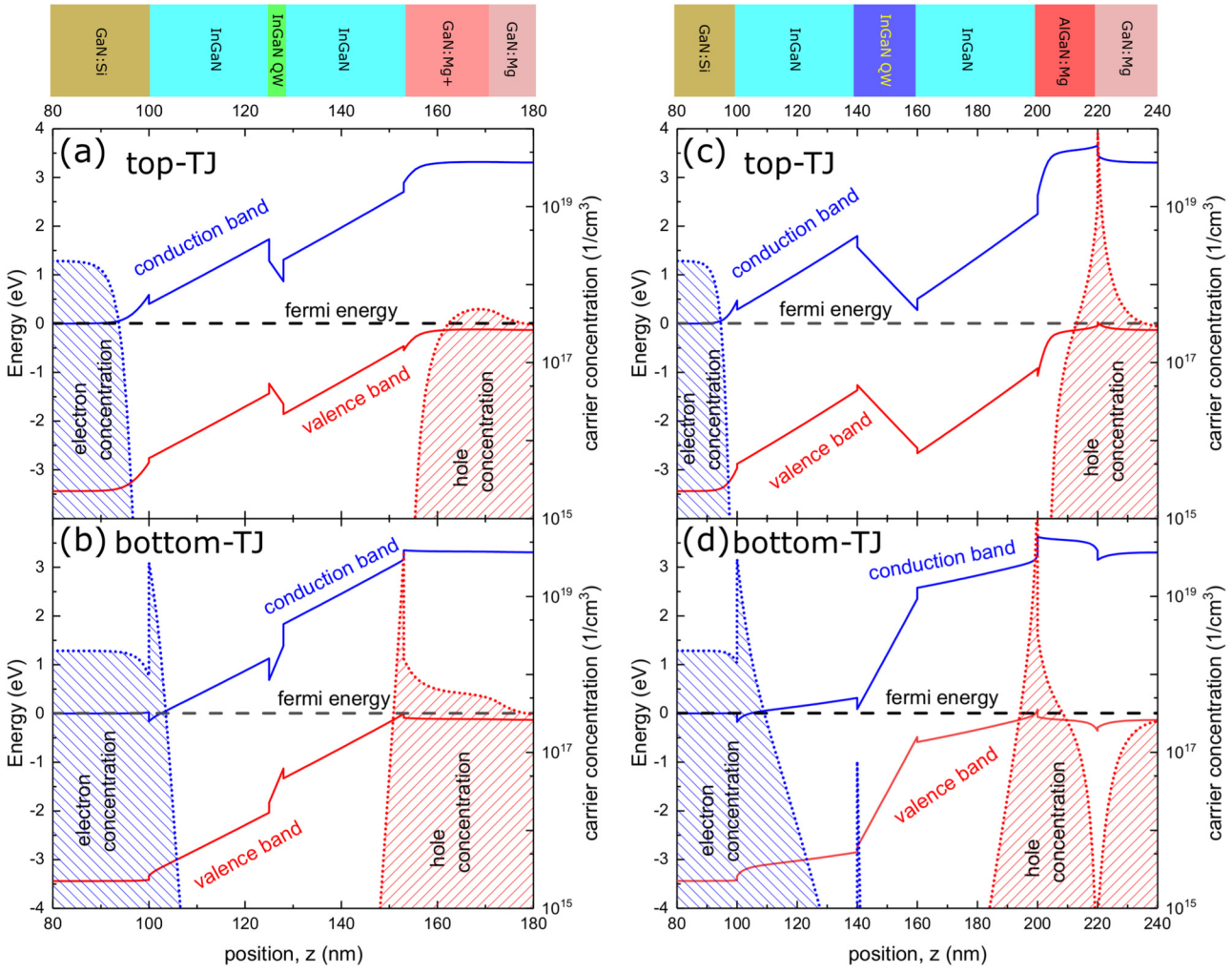

FIG. 9. Energy band diagrams with a carrier concentration at 0 V obtained using the SiLENSe package [(a)–(d)] comparing results obtained for structures A and B and structures C and D. The top-TJ blue LED has a triangular well at 140–160 nm that can trap charges. The bottom-TJ green and blue LEDs have smaller depletion regions.

at 0 V were performed. The calculated energy band diagrams and mobile carrier concentrations in the vicinity of the active regions of structures A, B, C, and D are shown in Figs. 9(a)–9(d), respectively. It is seen clearly that the polarization-induced electric field results in the thinning of the net depletion width for the bottom-TJ structures vs the top-TJ structures (seen for B vs A and D vs C). The peaks in the electron and hole concentrations near the active region that are present for the bottom-TJ LED structures are caused by the GaN/InGaN and InGaN/AlGaN heterojunction band offsets and promote better carrier injection into QW. The AlGaN/GaN interface that causes the peak in the hole concentration for structure C is on the other side of the EBL, leading to lower hole injection efficiency. The energy band diagrams also provide insight into the origins of the hysteresis observed in C-V for sample C. A deep triangular well is formed around 160 nm in the conduction band, with barriers on both sides. The hysteresis is caused by charging/discharging of this local, triangular minimum of the potential due to carriers injected or extracted from this region. The same barrier is responsible for blocking carrier injection into the QW at low currents, leading to a dominant parasitic high energy peak associated with emission from InGaN cladding layers in the EL spectra of Fig. 6(c). In the case of structure D, which also has a thick QW, the barrier for carrier escape is significantly smaller, leading to significantly lower hysteresis as seen in Fig. 8(b) for the bottom-TJ vs the top-TJ. Such carrier trapping in the top-TJ LEDs can be detrimental for fast electronic modulation of the LEDs or LDs, suggesting that the bottom-TJ construction is superior for such high-speed applications as in visual light communications (VLC) or LiFi (light-fidelity).

CONCLUSIONS

In this work, a fundamentally new approach of using bottom-tunnel junctions for polar GaN-based light-emitting diodes and lasers has been demonstrated. A clear experimental assessment of the impact of the polarization-induced electric fields and their relative orientation with the p-n diode junction fields on LED performance was possible for the first time with the bottom-TJ approach. Electroluminescence measurements on top-TJ and bottom-TJ LEDs emitting in blue as well as green-yellow spectrum indicate that the bottom-TJ LEDs achieve superior injection efficiency (in a Ga-polar p-down structure, which effectively mimics the desired N-polar p-up LED structure). Corroborating device simulations explain the experimental trends observed in the EL spectra such as higher emission intensities at high injection currents for bottom-TJ over top-TJ structures: the polarization-induced electric fields present in the bottom-TJ structures are in a direction that assists carrier injection, while effectively separating electrons and holes in the vicinity of the QW, suppressing parasitic carrier recombination. Further supporting capacitance-voltage measurements confirm the experimental observation of significantly thinner depletion widths and better injection efficiency for the bottom-TJ LEDs compared to the top-TJ counterparts. Based on the comparative study, we conclude that the bottom-TJ LEDs present an intriguing alternative to standard Ga-polar LEDs for achieving high efficiencies, monochromaticity, and for high frequency direct modulation of the photonic output. Combining the above advantages with the excellent current spreading by using a thick n-type GaN layer on the top, the first realization of a bottom-tunnel junction GaN LED presented here paves a new unexplored path for GaN-based photonic devices.

ACKNOWLEDGMENTS

This work was supported partially by the Polish National Centre for Research and Development (Grant Nos. LIDER/29/0185/L-7/15/NCBR/2016 and PBS3/A3/23/2015) during the visit of the lead author at Cornell University and the Foundation for Polish Science co-financed by the European Union under the European Regional Development Fund (Grant. No. POIR.04.04.00-00-5D5B/18-00). The work at Cornell University was supported in part by the following National Science Foundation (NSF) grants: NSF DMREF Award No. 1534303 monitored by Dr. J. Schluter, NSF Award No. 1710298 monitored by Dr. T. Paskova, NSF CCMR MRSEC Award No. 1719875, and NSF RAISE TAQs Award No. 1839196 monitored by Dr. D. Dagenais. The cleanroom fabrication at the Cornell Nanofabrication Facility (CNF) was supported in part by the NSF National Nanotechnology Coordinated Infrastructure (Grant No. ECCS-1542081).

REFERENCES

[1]S. Nakamura, Rev. Mod. Phys. **87**, 1139 (2015).
[2]*Polarization Effects in Semiconductors*, edited by C. Wood and D. Jena (Springer, 2008).
[3]D. Jena, J. Simon, A. K. Wang, Y. Cao, K. Goodman, J. Verma, S. Ganguly, G. Li, K. Karda, V. Protasenko, C. Lian, T. Kosel, P. Fay, and H. Xing, Phys. Status Solidi A **208**, 1511 (2011).
[4]S. Fernández-Garrido, J. Lähnemann, C. Hauswald, M. Korytov, M. Albrecht, C. Chèze, C. Skierbiszewski, and O. Brandt, Phys. Rev. Appl. **6**, 034017 (2016).
[5]T. K. Zywietz, J. Neugebauer, and M. Scheffler, Appl. Phys. Lett. **74**, 1695 (1999).
[6]C. Chèze, F. Feix, J. Lähnemann, T. Flissikowski, M. Kryśko, P. Wolny, H. Turski, C. Skierbiszewski, and O. Brandt, Appl. Phys. Lett. **112**, 022102 (2018).
[7]C. Chèze, M. Siekacz, G. Muzioł, H. Turski, S. Grzanka, M. Kryśko, J. L. Weyher, M. Boćkowski, C. Hauswald, J. Lähnemann, O. Brandt, M. Albrecht, and C. Skierbiszewski, J. Vac. Sci. Technol. B **31**, 03C130 (2013).
[8]F. Feix, T. Flissikowski, K. K. Sabelfeld, V. M. Kaganer, M. Wolz, L. Geelhaar, H. T. Grahn, and O. Brandt, Phys. Rev. Appl. **8**, 014032 (2017).
[9]V. Kirilyuk, A. R. A. Zauner, P. C. M. Christianen, J. L. Weyher, P. R. Hageman, and P. K. Larsen, J. Cryst. Growth **230**, 477 (2001).
[10]H. Masui, S. Keller, N. Fellows, N. A. Fichtenbaum, M. Furukawa, S. Nakamura, U. K. Mishra, and S. P. DenBaars, Jpn. J. Appl. Phys. **48**, 071003 (2009).
[11]M. J. Grundmann and U. K. Mishra, Phys. Status Solidi C **4**(7), 2830 (2007).
[12]A. T. M. Golam Sarwar, B. J. May, J. I. Deitz, T. J. Grassman, D. W. McComb, and R. C. Myers, Appl. Phys. Lett. **107**, 101103 (2015).
[13]S. M. Sadaf, Y. H. Ra, H. P. Nguyen, M. Djavid, and Z. Mi, Nano Lett. **15**, 6696 (2015).
[14]S. M. Sadaf, Y. H. Ra, T. Szkopek, and Z. Mi, Nano Lett. **16**, 1076 (2016).
[15]A. T. M. Golam Sarwar, S. D. Carnevale, T. F. Kent, F. Yang, D. W. McComb, and R. C. Myers, Appl. Phys. Lett. **106**, 032102 (2015).
[16]S. D. Carnevale, T. F. Kent, P. J. Phillips, A. T. Sarwar, C. Selcu, R. F. Klie, and R. C. Myers, Nano Lett. **13**, 3029 (2013).
[17]Y. Kuwano, M. Kaga, T. Morita, K. Yamashita, K. Yagi, M. Iwaya, T. Takeuchi, S. Kamiyama, and I. Akasaki, Jpn. J. Appl. Phys. **52**, 08JK12 (2013).
[18]W. Li, K. Nomoto, K. Lee, S. M. Islam, Z. Hu, M. Zhu, X. Gao, J. Xie, M. Pilla, D. Jena, and H. G. Xing, Appl. Phys. Lett. **113**, 062105 (2018).

[19]C. Skierbiszewski, G. Muziol, K. Nowakowski-Szkudlarek, H. Turski, M. Siekacz, A. Feduniewicz-Zmuda, A. Nowakowska-Szkudlarek, M. Sawicka, and P. Perlin, Appl. Phys. Express **11**, 034103 (2018).
[20]R. Czernecki, E. Grzanka, R. Jakiela, S. Grzanka, C. Skierbiszewski, H. Turski, P. Perlin, T. Suski, K. Donimirski, and M. Leszczynski, J. Alloys Compd. **747**, 354 (2018).
[21]C. Skierbiszewski, H. Turski, G. Muziol, M. Siekacz, M. Sawicka, G. Cywiński, Z. R. Wasilewski, and S. Porowski, J. Phys. D Appl. Phys. **47**, 073001 (2014).
[22]M. Malinverni, C. Tardy, M. Rossetti, A. Castiglia, M. Duelk, C. Vélez, D. Martin, and N. Grandjean, Appl. Phys. Express **9**, 061004 (2016).
[23]E. C. Young, B. P. Yonkee, F. Wu, S. H. Oh, S. P. DenBaars, S. Nakamura, and J. S. Speck, Appl. Phys. Express **9**, 022102 (2016).
[24]C. T. Foxon, R. P. Campion, V. A. Grant, S. V. Novikov, J. J. Harris, R. Thomson, C. Taylor, and D. Barlett, J. Cryst. Growth **301–302**, 482 (2007).
[25]H. Turski, M. Siekacz, Z. R. Wasilewski, M. Sawicka, S. Porowski, and C. Skierbiszewski, J. Cryst. Growth **367**, 115 (2013).
[26]H. Turski, G. Muzioł, M. Siekacz, P. Wolny, K. Szkudlarek, A. Feduniewicz-Żmuda, K. Dybko, and C. Skierbiszewski, J. Cryst. Growth **482**, 56 (2018).
[27]G. Muziol, H. Turski, M. Siekacz, K. Szkudlarek, L. Janicki, S. Zolud, R. Kudrawiec, T. Suski, and C. Skierbiszewski, preprint arXiv:1810.07612 (2018).
[28]J. Simon, Z. Zhang, K. Goodman, H. Xing, T. Kosel, P. Fay, and D. Jena, Phys. Rev. Lett. **103**, 026801 (2009).
[29]S. Krishnamoorthy, F. Akyol, P. S. Park, and S. Rajan, Appl. Phys. Lett. **102**, 113503 (2013).
[30]F. Akyol, S. Krishnamoorthy, Y. Zhang, J. Johnson, J. Hwang, and S. Rajan, Appl. Phys. Lett. **108**, 131103 (2016).
[31]X. Yan, W. Li, S. M. Islam, K. Pourang, H. Xing, P. Fay, and D. Jena, Appl. Phys. Lett. **107**, 163504 (2015).
[32]S. Krishnamoorthy, F. Akyol, and S. Rajan, Appl. Phys. Lett. **105**, 141104 (2014).
[33]F. Akyol, S. Krishnamoorthy, and S. Rajan, Appl. Phys. Lett. **103**, 081107 (2013).
[34]J. S. Kwak, S. E. Mohney, J.-Y. Lin, and R. S. Kern, Semicond. Sci. Technol. **15**, 756 (2000).
[35]J. Verma, J. Simon, V. Protasenko, T. Kosel, H. G. Xing, and D. Jena, Appl. Phys. Lett. **99**, 171104 (2011).
[36]H. Turski, R. Yan, S. J. Bader, G. Muzioł, C. Skierbiszewski, H. G. Xing, and D. Jena, "S-shaped negative differential resistance in III-nitride blue quantum-well laser diodes grown by plasma-assisted MBE," in *2017 75th Annual Device Research Conference (DRC), South Bend, IN, 25–28 June 2017* (IEEE, 2017), p. 1.
[37]H. Turski, M. Siekacz, M. Sawicka, G. Cywinski, M. Krysko, S. Grzanka, J. Smalc-Koziorowska, I. Grzegory, S. Porowski, Z. R. Wasilewski, and C. Skierbiszewski, J. Vac. Sci. Technol. B **29**, 03C136 (2011).
[38]K. Kojima, M. Funato, Y. Kawakami, H. Braun, U. Schwarz, S. Nagahama, and T. Mukai, Phys. Status Solidi C **5**, 2126 (2008).
[39]S. Y. Davydov, Phys. Solid State **51**, 1231 (2009).